

1 **Usability of one-class classification in mapping and detecting changes**
2 **in bare peat surfaces in the tundra**

3 Aleksi Räsänen, corresponding author

4 *Ecosystems and Environment Research Programme, Faculty of Biological and*
5 *Environmental Sciences, and Helsinki Institute of Sustainability Science (HELSUS),*
6 *PO Box 65, FI-00014 University of Helsinki, Finland, aleksi.rasanen@helsinki.fi*

7 *Department of Geography, Norwegian University of Science and Technology, NO-7491*
8 *Trondheim, Norway*

9 Vladimir Elsakov

10 *Institute of Biology of Komi Scientific Centre of the Ural Branch of the Russian*
11 *Academy of Sciences, Kommunisticheskaya, 28, Syktyvkar, Komi Republic, Russia,*
12 *elsakov@ib.komisc.ru*

13 Tarmo Virtanen

14 *Ecosystems and Environment Research Programme, Faculty of Biological and*
15 *Environmental Sciences, and Helsinki Institute of Sustainability Science (HELSUS),*
16 *PO Box 65, FI-00014 University of Helsinki, Finland, tarmo.virtanen@helsinki.fi*

17 word count: 10,357

18

19

20

21

22

23

24 **Usability of one-class classification in mapping and detecting changes** 25 **in bare peat surfaces in the tundra**

26 Arctic areas have experienced greening and changes in permafrost caused by
27 climate change during recent decades. However, there has been a lack of
28 automated methods in mapping changes in fine-scale patterns of permafrost
29 landscapes. We mapped areal coverage of bare peat areas and changes in them in
30 a peat plateau located in north-western Russia between 2007 and 2015. We
31 utilized QuickBird and WorldView-3 satellite image data in an object-based
32 setting. We compared four different one-class classifiers (one-class support
33 vector machine, binary support vector machine, random forest, rotation forest)
34 both in a fully supervised binary setting and with positive and unlabelled training
35 data. There was notable variation in classification performance. The bare peat
36 area *F*-score varied between 0.77 and 0.96 when evaluated by cross-validated
37 training data and between 0.22 and 0.57 when evaluated by independent test data.
38 Overall, random forest performed the most robustly but all classifiers performed
39 well in some classifications. During the 8 year period, there was a 21%–26%
40 decrease in the bare peat areal coverage. We conclude that (1) tested classifiers
41 can be used in one-class settings and (2) there is a need to develop methods for
42 tracking changes in single land cover types.

43 **Keywords:** Arctic, change detection, land cover, one-class classification, remote
44 sensing, very high spatial resolution

45 **1. Introduction**

46 Arctic areas in general and Arctic peatlands in particular have been heavily influenced
47 by recent global warming. It has been reported that the Arctic is greening, usually
48 meaning that the amount of green vegetation, especially bush coverage, is increasing in
49 tundra areas (Tape, Sturm and Racine 2006; Elmendorf et al. 2012; Myers-Smith et al.
50 2015; Yu et al. 2017), and that climate warming and geomorphic disturbances have
51 caused changes in permafrost areas (Beck et al. 2015; Segal, Lantz and Kokelj 2016;
52 Borge et al. 2017; Obu et al. 2017). It has been found that bare peat surfaces, the
53 identification of which is the target of our study, can be significant nitrous oxide, carbon

54 dioxide and methane sources in the tundra (Repo et al. 2009; Marushchak et al. 2011;
55 Voigt et al. 2016). Furthermore, their areal coverage seems to be dynamic in time and
56 their abundance in the Arctic is still poorly known (Repo et al. 2009; Marushchak et al.
57 2011; Voigt et al. 2016).

58 Remote sensing methods are widely used in mapping Arctic land cover and
59 permafrost (Pflugmacher et al. 2011; Westermann et al. 2014; Bartsch et al. 2016) and
60 tracking changes in land cover patterns (Singh 1989; Stow et al. 2004; Beck et al. 2015;
61 Tewkesbury et al. 2015; Jorgenson and Grosse 2016). Due to fine-scale heterogeneity in
62 thermokarst and tundra environments, very high spatial resolution (VHSR, spatial
63 resolution < 5.00 m) satellite images are needed to map the extent and spatial patterns of
64 small land cover patches such as bare peat surfaces (Laidler and Treitz 2003; Belshe,
65 Schuur and Grosse 2013; Virtanen and Ek 2014). It has been argued that more high-
66 resolution studies are needed to map changes in Arctic environments, and there is a
67 need to develop standardized methods for tracking the changes (Jorgenson and Grosse
68 2016).

69 There are some but not many previous studies evaluating fine-scale changes in
70 permafrost landscapes. Borge et al. (2017) combined visual interpretation with an
71 analysis of climate data when they evaluated the decrease in palsa mires in northern
72 Norway. Similarly, visual interpretation has been used in the mapping of changes in
73 thermokarst lakes and lithalsas in Quebec (Beck et al. 2015) and in thaw slump activity
74 in the western Canadian Arctic (Segal et al. 2016). While these studies have
75 incorporated visual interpretation, there has been a lack of automated approaches for
76 mapping changes in fine-scale patterns of single land cover classes.

77 To map patches of single land cover classes, there has been a recent rise in the
78 use of one-class, binary and positive and unlabelled (PU) classification methods as

79 opposed to multi-class classification methods (Boyd, Sanchez-Hernandez and Foody
80 2006; Sanchez-Hernandez, Boyd and Foody 2007; Li and Guo 2010; Li, Guo and Elkan
81 2011; Mack, Roscher and Waske 2014; Baldeck and Asner 2015; Baldeck et al. 2015;
82 Barbosa et al. 2016; Chen et al. 2016; Mack et al. 2016; Song et al. 2016; Mack and
83 Waske 2017; Stenzel et al. 2017; Araya-López et al. 2018; Deng et al. 2018; Liu et al.
84 2018). In one-class classification, training data are needed only for the focal class (i.e.
85 presence data). This makes it easier to use than multi-class classification in which
86 training data are needed for all classes. In PU classifications, there are also training data
87 for unlabelled (so-called pseudo-outlier) points, whereas binary classifiers are
88 performed in a one-against-all setting.

89 Typical methods in one-class, PU and binary classification include support
90 vector machines (SVMs) (Boyd et al. 2006; Sanchez-Hernandez et al. 2007; Baldeck
91 and Asner 2015; Mack et al. 2016; Stenzel et al. 2017), a maximum entropy approach
92 (Maxent) (Li and Guo 2010; Lin et al. 2014; Stenzel et al. 2014; Amici et al. 2017;
93 Andrew and Shephard 2017; Stenzel et al. 2017; Chignell et al. 2018; Noviello et al.
94 2018), as well as PU and presence and background learning algorithms (Li et al. 2011;
95 Xu et al. 2016; Ao et al. 2017; Deng et al. 2018; Liu et al. 2018). Also, regression
96 methods such as random forest (RF) and boosted regression trees have been used in
97 mapping the presence of single land cover types (Chignell et al. 2018), while state-of-
98 the-art classification methods other than SVMs, Maxent and PU learning have been
99 little used.

100 SVM is a non-parametric statistical learning technique in which observations are
101 divided into classes with the help of hyperplanes (Vapnik 1982; Mountrakis, Im and
102 Ogole 2011). In one-class SVM (OCSVM), only positive data are used in the training of
103 the classifier; in biased SVM, PU data are used, and positive data are given a larger

104 misclassification cost; and in binary SVM, data from two classes are used (Baldeck and
105 Asner 2015; Baldeck et al. 2015; Barbosa et al. 2016; Mack et al. 2016; Mack and
106 Waske 2017; Stenzel et al. 2017). Maxent is a one-class machine learning method in
107 which relative entropy between two probability densities (i.e. presence data and
108 environmental covariates) is trying to be minimized (Elith et al. 2011). Maxent has been
109 typically used in the modelling of suitable habitats or species distributions of specific
110 species using remote sensing and other data (Phillips, Anderson and Schapire 2006;
111 Elith et al. 2011), but it has also been used in other kinds of remote sensing tasks, such
112 as mapping archaeological sites (Noviello et al. 2018), eagle nests (Andrew and
113 Shephard 2017) and habitat types (Stenzel et al. 2014; Chignell et al. 2018). As the
114 name of the method indicates, the PU learning algorithm uses PU data in model
115 building. The PU learning algorithm is carried out in two steps: the model is first trained
116 with PU data, and a specific constant factor is estimated from validation data (Li et al.
117 2011). PU learning needs to be implemented with a classification algorithm that can
118 estimate conditional probabilities. Usually, PU has been implemented with back-
119 propagation neural networks (Li et al. 2011; Xu et al. 2016; Ao et al. 2017; Deng et al.
120 2018) but also model comparisons have been conducted (Liu et al. 2018).

121 When comparing different classification algorithms, it has been found that
122 biased and binary SVMs in particular are promising methods for mapping patches of
123 rare habitat type (Boyd et al. 2006; Sanchez-Hernandez et al. 2007; Mack et al. 2016;
124 Stenzel et al. 2017) and that they usually outperform other one-class classification
125 methods (Boyd et al. 2006; Baldeck and Asner 2015; Baldeck et al. 2015; Barbosa et al.
126 2016; Mack and Waske 2017; Stenzel et al. 2017). In some comparisons against biased
127 or binary SVMs, slightly higher classification accuracy has been achieved with iterative

128 biased SVM (Mack et al. 2016) and the PU learning algorithm (Li et al. 2011; Xu et al.
129 2016; Ao et al. 2017; Deng et al. 2018; Liu et al. 2018).

130 Here, we address three gaps in the remote sensing literature. First, we assess
131 one-class classification in tracking fine-scale changes in tundra environments, which
132 have been studied relatively little. Second, there have been few attempts to use one-
133 class and PU classification methods to track changes, and these studies have employed
134 Maxent (Lin et al. 2014; Amici et al. 2017) or OCSVM (Li and Xu 2010) in rather
135 coarse resolution mapping. Here, we map fine-scale changes in bare peat surfaces in
136 Russian tundra using VHSR satellite images at two time points (2007 and 2015). Third,
137 although there has been a notable increase in one-class, biased and binary
138 classifications, there has been little evaluation of how methods other than SVM, Maxent
139 and PU learning handle the binary and PU classification situations. Hence, we test the
140 performance of RF and rotation forest (ROF) against binary/biased SVM (BSVM) and
141 OCSVM. We evaluate these methods in an object-based setting by comparing fully
142 supervised binary classification (i.e. peat surfaces against all other land cover classes)
143 with PU classification in which we used training data from bare peat areas and
144 unlabelled random points.

145 **2. Materials and methods**

146 ***2.1. Study area and bare peat surfaces***

147 Our study area is in the Seida peat plateau (67°04'00"N, 62°55'00"E, Figure 1) located
148 in a discontinuous permafrost zone in the Usa River Basin in the north-eastern corner of
149 European Russia, 70 km south-west of the town of Vorkuta. The area is characterized
150 by low Arctic shrub vegetation and lies just north of the tree line. The mean annual
151 temperature in the region is approximately -6 °C and the annual precipitation is just

152 above 505 mm (Repo et al. 2009; Marushchak et al. 2011; Hugelius et al. 2012; Voigt et
153 al. 2016). The area is composed of a mosaic of peat plateaus, mineral moraine deposits,
154 and thermokarst lakes. Peat plateaus with permafrost bogs and fens rise above the
155 surrounding landscape due to high ground ice content, and the peat layer is in many
156 locations over 4 m thick (Hugelius et al. 2012).

157 **FIGURE 1 APPROXIMATELY HERE**

158 We tracked the areal coverage and changes in the extent of bare peat surfaces,
159 whose coverage has been estimated to be around 1% of the peat plateau (Marushchak et
160 al. 2013). These surfaces have been developed by late Holocene permafrost aggradation
161 (Väliranta et al. 2018), wind erosion (Seppälä 2003) and soil mixing due to frost action,
162 i.e. cryoturbation (Bockheim and Tarnocai 1998; Peterson and Krantz 2003; Repo et al.
163 2009). According to recent findings, the surfaces are remnants of larger non-vegetated
164 areas in the past (Väliranta et al. 2018). Bare peat surfaces are of two types. Peat circles
165 are flat surfaces with no vascular plants but are partly covered by thin moss and algal
166 crust. Peat mounds are drier than peat circles and partly vegetated by lichens and
167 graminoids. Peat mounds do not have a frozen core but are located within a frozen peat
168 plateau (Marushchak et al. 2011).

169 ***2.2. Used data***

170 In the classifications, we used two VHSR satellite images taken during different
171 growing seasons. The first one was a QuickBird (QB) image (DigitalGlobe,
172 Westminster, CO, USA) with 2.40 m spatial resolution and four bands (blue, green, red,
173 near-infrared) taken on 6 July 2007. The second one was a WorldView-3 (WV-3) image
174 (DigitalGlobe, Westminster, CO, USA) with 1.60 m spatial resolution and eight bands
175 (coastal blue, yellow, red-edge and near-infrared 2 in addition to the QB bands) taken
176 on 9 August 2015. We first atmospherically corrected both images using the dark-object

177 subtraction method (Chavez 1988) and then georeferenced them to match the field data
178 and each other.

179 To acquire the ground reference data, we used (1) visual interpretation of
180 satellite images and (2) a DJI (Dà-Jiāng Innovations) Phantom 2 Vision Plus drone
181 image with 0.04 m resolution taken on 2 August 2015 as well as (3) fieldwork data sets
182 from July–August 2007 and 2016. The mosaic of drone images (nearly 615 images) was
183 developed using Agisoft PhotoScan software (Agisoft, St Petersburg, Russia). In the
184 fieldwork, we collected data mostly for a purpose other than mapping bare peat areas
185 but got a good overall view of the bare peat areas and received help in how they could
186 be interpreted from satellite images.

187 ***2.3. Overview of the classification approach***

188 It has been shown that object-based methods are more applicable than pixel-based
189 methods in classifying VHSR images (Blaschke et al. 2014). Therefore, we employed
190 an object-based classification approach in which we first segmented images and then
191 classified them in two different settings (Figure 2). In the first classification setting, we
192 carried out a fully supervised binary classification and in the second setting, we
193 classified the image with the help of PU segments (PU classification setting). In both
194 settings, we tested four different classifiers and reduced the number of features using a
195 feature selection algorithm. Finally, we assessed classification accuracy in a different
196 area than the training area. Classifications were carried out separately for the QB and
197 WV-3 images. For WV-3, we carried out two classification alternatives: a low-
198 resolution (we use the acronym WV-3LR) version with data resampled at 2.40 m
199 ground resolution and four bands identical to QB classification, and a high-resolution
200 (WV-3HR) version with 1.60 m resolution and all eight bands.

201 **FIGURE 2 APPROXIMATELY HERE**

202 *2.4. Image segmentation*

203 We segmented images using full lambda schedule (FLS) segmentation in Erdas Imagine
204 2014 (Intergraph, Madison, AL, USA). FLS segmentation is a region-based
205 segmentation in which pixels are merged with their neighbouring pixels if certain
206 conditions are met. FLS uses spectral (mean pixel value in the segment), textural
207 (standard deviation of pixel values in the segment), shape (areal complexity of the
208 segment) and size information when decisions about merging are carried out. This
209 information can be given relative weights. Furthermore, the average size of the segment
210 (i.e. pixel/segment ratio) and the minimum and maximum segment sizes can also be
211 adjusted.

212 We parameterized segmentations with the help of visual interpretation as it is
213 often the most meaningful method for segmentation evaluation in natural environments
214 (Räsänen et al. 2013). When setting the parameters, we had three objectives: (1) the
215 segments should be as large as possible, but (2) even the smaller bare peat areas should
216 be delineated, and (3) the average size of the segment should be the same for all
217 classifications. We ended up giving weights of 0.7, 0.5, 0.3 and 0.3 to spectral, textural,
218 shape and size information respectively. Hence, we gave the largest relative weight to
219 spectral information as the bare peat surfaces usually have a distinct colour in the
220 images. We set the pixel/segment ratio to 50 for 2.40 m resolution classifications and to
221 112 for the 1.60 m resolution classification, and we gave minimum and maximum
222 segment sizes the default values of 10 and 2000 respectively.

223 *2.5. Calculated features*

224 For each segment and image band, we calculated 34 features using package EBImage
225 (Pau et al. 2010) in R 3.2.2 (R Core Team 2015). To analyse texture, we calculated the

226 following 13 grey-level co-occurrence matrix (GLCM) features: angular second
227 moment, contrast, correlation, sum of squares: variance, inverse difference moment,
228 sum average, sum variance, sum entropy, entropy, difference variance, difference
229 entropy, and two information measures of correlation (Haralick, Dinstein and
230 Shanmugam 1973) which are among the most widely used textural features (Benz et al.
231 2004; Pacifici, Chini and Emery 2009; Blaschke et al. 2014). When calculating the
232 GLCM features, we quantized data to 32 levels. We calculated all GLCM features at
233 two scales; in other words, we calculated the adjacency of pixels to their closest and
234 second closest neighbouring pixels. In addition, we calculated mean, standard deviation,
235 mean absolute deviation, and 1%, 5%, 50%, 95% and 99% quantiles. We calculated
236 features from each image band as well as from three band indices: normalized
237 difference vegetation index (NDVI, Rouse et al. 1973), red-green index (RGI, Coops et
238 al. 2006) and normalized difference water index (McFeeters 1996). Hence, we ended up
239 with 374 features for the WV-3HR classification and 238 features for the QB and WV-
240 3LR classifications.

241 ***2.6. Classification settings***

242 We used two classification settings: binary and PU. For the binary classification, we
243 manually classified an area of the images for bare peat segments and other segments.
244 We carried out this classification in the area where most of the fieldwork in 2016 was
245 conducted. We used our knowledge of the terrain collected during the fieldwork and
246 visual interpretation of the VHSR images when constructing the training data. In binary
247 classifications, we ended up with 122 (WV-3HR), 92 (WV-3LR) and 98 (QB) segments
248 for the bare peat class, and 1112 (WV-3HR), 1027 (WV-3LR) and 1067 (QB) for the
249 other class (Figure 3). For the PU classification, we used the same bare peat areas as for
250 the binary classification. For the unlabelled points, we randomly drew 1000 segments

251 from the overall study area.

252 FIGURE 3 APPROXIMATELY HERE

253 *2.7. Used classifiers and their parameterization*

254 We used four different classifiers: OCSVM, BSVM, ROF and RF in both classification
255 settings.

256 SVMs have been used widely in binary, PU and one-class settings, and BSVM
257 has performed the best in various comparisons (Baldeck and Asner 2015; Baldeck et al.
258 2015; Barbosa et al. 2016; Mack and Waske 2017; Stenzel et al. 2017). In SVMs,
259 observations are divided into a discrete number of classes with the help of hyperplanes,
260 and the closest training samples to the hyperplanes are called support vectors (Vapnik
261 1982; Mountrakis et al. 2011). In its simplest form, SVM is a linear binary classifier.
262 However, there are also techniques such as kernels that modify hyperplanes so that
263 separability between classes does not need to be linear and also further adjustments that
264 enable classification into multiple classes (Mountrakis et al. 2011). SVM generally
265 needs only small training data sets and handles multidimensional data sets making it
266 appealing for remote sensing classification tasks (Mountrakis et al. 2011). We used a
267 radial basis function kernel (Vert, Tsuda and Schölkopf 2004) when conducting SVM
268 classifications in one-class, biased and binary settings. SVMs are sensitive to changes in
269 parameter values and typically a grid search is used in parameterization (Mack et al.
270 2014; Baldeck and Asner 2015; Baldeck et al. 2015; Barbosa et al. 2016; Mack et al.
271 2016; Mack and Waske 2017; Stenzel et al. 2017).

272 OCSVM uses only data from the positive class and searches for the optimal
273 configuration that separates the positive class (Schölkopf et al. 2000). In OCSVM with
274 radial basis function kernel, two parameters need to be set: inverse kernel width (σ)
275 (Vert et al. 2004) and the upper bound for the training error (ν) (Schölkopf et al. 2000).

276 After initial evaluation we tested the following parameter values: $\sigma \in \{1 \times 10^{-7}, 1 \times 10^{-6},$
277 $\dots, 1 \times 10^{-2}\}$ and the upper bound for the training error $\nu \in (0.01, 0.05, 0.10, \dots, 0.25)$.

278 Binary and biased SVM use data from two classes in training. In binary SVM, it
279 is known that training samples originate from two different classes. The classifier tries
280 to maximize the distance between the hyperplane and support vector and minimize
281 misclassifications. Misclassifications are penalized using a cost parameter (C) (Vapnik
282 1982). In biased SVM, unlabelled samples may include samples from the positive class
283 (Liu et al. 2003). Therefore, two classes are given a different weight through C ;
284 misclassifications of the focal class are penalized more than misclassifications in the
285 unlabelled samples using an extra cost parameter $C+$ (Liu et al. 2003). We tested the
286 following parameter values with BSVM: $\sigma \in \{1 \times 10^{-7}, 1 \times 10^{-6}, \dots, 1 \times 10^{-2}\}$, $C \in \{1 \times$
287 $10^3, 1 \times 10^4, \dots, 1 \times 10^7\}$ and $C+ \in \{1 \times 10^0, 1 \times 10^1, \dots, 1 \times 10^5\}$. We thus allowed
288 equal misclassification costs for both classes. For both OCSVM and BSVM, we tuned
289 parameters using tenfold cross-validation.

290 RF has generally performed well in various comparisons and it is capable of
291 handling multidimensional data (Duro, Franklin and Dubé 2012; Rodriguez-Galiano et
292 al. 2012; Adam et al. 2014; Belgiu and Dragut 2016). It is an ensemble classifier which
293 combines multiple bootstrapped classification trees, and final classification is based on
294 a majority vote over all trees. When a tree is built, two thirds of the data are used for
295 training and the rest is used for evaluation and is called out-of-bag data. At each tree
296 node, the best split is chosen among a randomized subset of input features and the
297 number of tested features can be adjusted (Breiman 2001). In order to deal with
298 imbalanced data, one can increase the misclassification cost of a specific class by giving
299 a higher value to the class weight (W) parameter (Chen, Liaw and Breiman 2004). We
300 tuned W using out-of-bag assessment. After initial testing to find a suitable range for the

301 positive class W , we tested the following values: $W \in \{1 \times 10^5, 2 \times 10^5, \dots, 19 \times 10^5\}$.
302 Otherwise, RF has been found to be insensitive to parameterization (Rodriguez-Galiano
303 et al. 2012; Du et al. 2015), which we also verified in our initial evaluations. Thus, we
304 used the default values for the other parameters. We set the number of trees grown to
305 500 and the number of parameters tested in each node to the square root of the total
306 number of variables.

307 ROF has proven to be an efficient method for classifying remote sensing data
308 (Kavzoglu and Colkesen 2013) and it has outperformed SVM and RF in some
309 comparisons (Du et al. 2015). ROF is also an ensemble classifier of multiple
310 classification trees. In each tree, features are randomly split into subsets, and principal
311 component analysis is conducted for each subset so that the full feature set can be
312 reconstructed with subset axis rotation. Confidence for each class is calculated using an
313 average combination over all trees, and samples are assigned to the class with the
314 highest confidence (Rodriguez and Kuncheva 2006). Similarly to RF, ROF is insensitive
315 to parameterization (Du et al. 2015), and we verified this when testing the classifier. We
316 thus used default parameter values; in more detail, we chose the number of variable
317 subsets so that there were three features in each subset, and we set the number of trees
318 to ten.

319 For SVMs and RF, we chose the best parameter values based on the F -score,
320 which has been found to be applicable in binary and one-class classification settings
321 (Baldeck and Asner 2015; Baldeck et al. 2015). We conducted classifications in R 3.2.2
322 (R Core Team 2015) using packages `oneClass` (Mack et al. 2014), `randomForest` (Liaw
323 and Wiener 2002) and `rotationForest` (Ballings and Van der Poel 2015).

324 ***2.8.Feature selection***

325 In previous studies, it has been found that feature selection improves the classification
326 accuracy in SVM and RF classifications (Low et al. 2013; Rasanen et al. 2014; Li, XJ et
327 al. 2016). For selecting features, we used the RF wrapper algorithm Boruta (Kursa and
328 Rudnicki 2010) in R 3.2.2 (R Core Team 2015). Boruta and other RF-based feature
329 selection are compatible with SVMs (Low et al. 2013; Li, XJ et al. 2016) and have
330 performed well in different comparisons (Samsudin et al. 2015; Li, Tran and Siwabessy
331 2016; Poona et al. 2016). Boruta feature selection proceeds as follows. Before each RF
332 run, shadows for each feature are created. Shadow feature values are obtained by
333 disarranging the values of the original feature across samples. After the run, the features
334 which have significantly lower importance than the shadow feature with the highest
335 importance are judged to be unimportant, and features having significantly higher
336 importance are judged important. Unimportant features are removed from the following
337 runs and Boruta ends when all features are deemed either important or unimportant or
338 when the maximum amount of RF runs have been conducted (Kursa and Rudnicki
339 2010), which in our case was after 1000 runs. For those variables which were still
340 tentative after 1000 runs, we carried out a tentative rough fix in which the median
341 importance of tentative features was compared with the median importance of the most
342 important shadow feature (Kursa and Rudnicki 2010).

343 ***2.9.Accuracy assessment and change detection***

344 We tested the accuracy of the classifications in an area covered by the drone image. In
345 constructing the reference against which classifications were evaluated, we visually
346 interpreted the drone image and delineated all bare peat areas with $> 20 \text{ m}^2$ extent. In
347 addition, we visually estimated whether the bare peat areas visible in the drone image

348 could be seen in the satellite images. We evaluated the performance of the methods by
349 both pixel-based and object-based metrics. First, we calculated the user's accuracy (i.e.
350 precision, the likelihood that the mapped area is a bare peat surface) and the producer's
351 accuracy (i.e. recall, the proportion of correctly classified bare peat surfaces). We also
352 calculated the *F*-score (i.e. the harmonic mean of the user's and producer's accuracy)
353 based on (1) the test data and (2) the out-of-bag (RF) or tenfold cross-validated (other
354 classifiers) estimate on the training data. Furthermore, we calculated the proportion of
355 positively classified segments having at least 10% and 50% bare peat coverage based on
356 the reference data. Then, we calculated the proportion of bare peat patches in the
357 reference of which 10% or 50% were classified as bare peat surfaces in the remote
358 sensing classifications. Finally, we calculated the number and areal coverage of bare
359 peat surfaces in the validation area based on each classifier and the reference, and in the
360 whole 10.9 km² study area of which approximately 5.5 km² is peat plateau (see
361 Hugelius et al. 2012 for the peat plateau area).

362 To track changes in bare peat areal coverage, we compared QB and WV-3LR
363 classifications, since they had similar spectral and spatial resolutions. We compared the
364 areal coverage and number of bare peat area patches in the whole study area using the
365 following metrics. First, we calculated the consensus of 3, 5 and 7 classifiers; in other
366 words, we mapped those segments that were classified as bare peat based on the
367 prediction of 3, 5 or 7 classifiers. Second, we calculated the average values of areal
368 coverage and number of patches over all classifications and reported also the lowest and
369 highest estimate of single classifiers.

370 3. Results

371 3.1. Feature and parameter selection

372 The Boruta feature selection reduced the number of features to 88, 80, 66, 54, 78 and 81
373 for the binary and PU QB, binary and PU WV-3LR, and binary and PU WV-3HR
374 classifications respectively. Features deemed important consisted usually of GLCM sum
375 average, GLCM sum variance, and mean and quantile features. Furthermore, features
376 calculated from the NDVI, RGI and the near-infrared band in the QB and WV-3LR
377 classifications, and features calculated from the red-edge band, NDVI and RGI followed
378 by red, green, and near-infrared 1 bands in the WV-3HR classifications were over-
379 represented in the final set of features. Nevertheless, some features from all bands were
380 included and all types of features were included in the final classifications.

381 In OCSVM classifications, the optimal value for σ varied between 1×10^{-4} and 1
382 $\times 10^{-3}$ and for ν between 0.01 and 0.15. In BSVM classifications, the optimal value for σ
383 varied between 1×10^{-7} and 1×10^{-3} , for C between 1×10^3 and 1×10^5 , and for $C+$
384 between 1×10^0 and 1×10^5 , but in most of the classifications, $C+$ was 1×10^0 . In all
385 BSVM classifications, F -scores close to the best F -score were obtained with several
386 parameter combinations including higher values for $C+$. In RF classifications, the
387 optimal W varied between 1×10^5 and 10×10^5 .

388 3.2. Classification and change detection

389 When looking at the cross-validation or out-of-bag performance of the training data, F -
390 scores for the different classifications varied between 0.77 and 0.96, with the highest F -
391 scores for ROF and lowest for OCSVM (Table 1). However, the F -scores were notably
392 smaller (0.22–0.57) when independent test data were used (Table 1). In the six
393 comparisons based on test data, RF had the highest F -score in five cases. The

394 classification accuracies were the highest for WV-3HR classifications and the lowest for
395 WV-3LR classifications, while the situation was the opposite in the evaluation based on
396 cross-validated training data.

397 TABLE 1 APPROXIMATELY HERE

398 There was considerable variation in the classifier performance based on
399 independent test data. All classifiers performed well in some classifications but not as
400 well in some other classifications (Tables 2 – 4). User accuracies varied between 22%
401 and 64% and producer accuracies between 22% and 60%. OCSVM had high producer
402 accuracies and low user accuracies especially in QB classifications and suffered thus
403 from over-classification in some cases. BSVM was more prone to under-classification
404 but it performed well especially in the PU WV-3 classifications. RF performed the most
405 robustly of the classifiers but had some under-prediction problems in the WV-3LR
406 classifications. ROF performed quite poorly in the WV-3LR classifications and under-
407 predicted in some classifications but had also high classification accuracies in other
408 classifications. In visual interpretation, the performance of the classifiers varied, and all
409 classifiers produced visually acceptable classifications (Figure 4).

410 TABLE 2 APPROXIMATELY HERE

411 TABLE 3 APPROXIMATELY HERE

412 TABLE 4 APPROXIMATELY HERE

413 FIGURE 4 APPROXIMATELY HERE

414 According to the consensus of five classifiers and average estimates, the number
415 of bare peat areas as well as their areal coverage decreased by 21%–26% between 2007
416 and 2015 (Table 5). Nevertheless, there was some under-prediction in many of the WV-
417 3LR classifications (Table 3). WV-3HR gave a similar area estimate and higher patch
418 number estimate than WV-3LR of on average 5.3 ha (4.5 ha – 7.8 ha) in 554 patches

419 (319–951), which could be judged as a better estimate due to higher classification
420 accuracy. Overall, the areal coverage of bare peat was around 0.5% of the study area
421 and 1.0% of the peat plateau.

422 TABLE 5 APPROXIMATELY HERE

423 4. Discussion

424 According to our results, there was considerable variation in classifier performance.
425 Although the *F*-scores were high when evaluated using cross-validated training data,
426 they were low when using independent test data. Actually, the cross-validated *F*-scores
427 were similar to the *F*-scores or accuracies received in some other studies using one-class
428 or binary classifications in relatively simple classification tasks in urban or agricultural
429 areas (Mack et al. 2014; Ao et al. 2017; Deng et al. 2018). On the other hand, the
430 classifier performance based on independent test data was comparable to earlier
431 classifier performance in more challenging classification tasks in natural environments
432 (Baldeck and Asner 2015; Stenzel et al. 2017), although higher classification accuracies
433 have also been obtained in natural environments (Baldeck et al. 2015; Mack et al.
434 2016). The reason for the high disparity between the classification accuracies can be
435 related to the fact that training data and test data were derived from different areas.
436 Although the distance between the areas is only 1 km – 2 km, the composition of land
437 cover classes is to some extent different. Another possibility would have been to use
438 part of the data from both areas for training and part of the data for testing. However, in
439 that case, we could not have used the drone image and manually delineated bare peat
440 areas in the test data, and we could only have used object-based metrics when
441 evaluating classifier performance. We judge the classifier performance based on the test
442 data as a more reliable estimate, because independent test data are usually
443 recommended (Mack and Waske 2017; Liu et al. 2018). Later in this section, we mostly

444 discuss the classifier performance against the independent test data.

445 When evaluated using the independent test data, RF performed most robustly in
446 classifying bare peat areas, and its performance was often slightly better than OCSVM
447 or BSVM. Quite surprisingly, the performance of OCSVM was approximately on par
448 with BSVM when evaluated using independent test data, which is in contrast to
449 previous research (Li et al. 2011; Baldeck and Asner 2015; Baldeck et al. 2015; Barbosa
450 et al. 2016; Ao et al. 2017; Mack and Waske 2017; Stenzel et al. 2017; Deng et al.
451 2018). However, the performance of OCSVM was lower compared with other
452 classifiers when evaluated by the cross-validated training data. It is also notable that
453 OCSVM produced different classification results in binary and PU settings, although it
454 uses only positive data for training. These dissimilarities were probably caused by
455 different final parameter sets.

456 In previous research, there has been mixed evidence as to whether there are
457 differences in classifier performance when comparing binary and PU settings. In one
458 comparison, higher classification accuracy has been achieved with binary SVM
459 compared with biased SVM (Mack et al. 2016); in a second comparison, the situation
460 was the opposite (Baldeck et al. 2015); and in a third comparison, the difference was
461 small between the two classifiers (Baldeck and Asner 2015). According to our results,
462 there was no clear trend in classifier performance between binary and PU settings.
463 Although there were divergences in single classifiers, equally high classification
464 accuracies could be achieved in both settings. Overall, we judge that all tested
465 classifiers can be used both in binary and PU settings, and especially RF showed
466 promising performance. Therefore, the use of the PU classification setting for all tested
467 classifiers can be recommended for future studies as this setting requires training data
468 only for the positive class.

469 Considering change detection, our results indicate that there has been a drastic
470 decrease in bare peat areas during the last decade. Based on all comparisons, the areal
471 coverage and number of bare peat surfaces is decreasing in the area. The detected
472 decrease can be related many factors which include an actual decrease in the number
473 and size of patches, a decrease in the number of patches that could be clearly identified
474 (i.e. segmented and classified), uncertainties in classifications such as under-prediction
475 in WV-3LR classifications, and goodness of the training data. Actually, already in
476 training data of the WV-3 classifications, the areal coverage of bare peat was 16% lower
477 than in the training data of the QB classification. Overall, the decrease is supported by
478 our field observations. We have observed that vegetation density and area covered by
479 vegetation seem to be at least to some extent increased around bare peat surfaces, and
480 there seem to be no new bare peat areas. The decrease is also supported by the recent
481 evidence that current bare peat areas are remnants of larger zones of barren land
482 (Väliranta et al. 2018) and by the observations that Arctic areas are greening (Tape et al.
483 2006; Elmendorf et al. 2012; Myers-Smith et al. 2015; Yu et al. 2017). On the other
484 hand, there has been little change in thermokarst lake coverage near the study site
485 between the mid-1970s and mid-2000s (Sannel and Kuhry 2011), which might mean
486 that there has been little change in the landscape dynamics also in our study area. It
487 might also be possible that bare areas would at some time also increase, at least
488 temporarily, if a warming climate creates quick disturbances to vegetation due to
489 changes in permafrost conditions in the area.

490 In earlier research, change detection in permafrost environments has been
491 concentrated on coarse-scale patterns, while fine-scale changes have been mostly
492 tracked with visual interpretation (Jorgenson and Grosse 2016). Nevertheless, as visual
493 interpretation is labour demanding, we urge for the development of an efficient and

494 automatic change tracking method for VHSR images. Furthermore, images could be
495 fused with repeat lidar analysis, which has been successfully used in tracking changes
496 (Jorgenson and Grosse 2016). Another possible avenue could be testing the resolution
497 requirements in tracking changes; in other words, what kind of changes that can be
498 detected using different resolution data sets could be assessed. In addition to
499 methodological developments, more validation studies with thorough field assessments
500 are needed to track fine-scale changes in permafrost environments.

501 There is a one-month difference in the timing of the QB and WV-3 images;
502 therefore, phenology might affect the classification of bare peat areas. Although there
503 are no phenological changes in non-vegetated surfaces such as bare peat, phenology
504 affects the interpretation of other land cover classes and vegetation types (Anderson et
505 al. 2016; Wang et al. 2016; Juutinen et al. 2017). This might then have a minor
506 influence on the classification of bare peat.

507 Our results show that the higher spectral and spatial resolution of WV-3HR
508 classifications gave higher classification accuracies than QB or WV-3LR
509 classifications. Also in earlier studies, it was found that WV-3 performs better than QB
510 in various environments (Novack et al. 2011; McCarthy and Halls 2014). Overall, WV-
511 3HR classifications were the most reliable in our case and showed that high spectral and
512 spatial resolution is needed in the mapping of bare peat areas.

513 **5. Conclusion**

514 To sum up, both binary and PU classification methods were shown to be appropriate in
515 mapping bare peat surfaces, but there were significant differences in classifier
516 predictions of bare peat areas. RF was the most robust classifier in the comparison, but
517 differences between classifiers were generally small. More research is needed in
518 evaluating the performance of RF and ROF in various one-class tasks and also in

519 evaluating whether single classes are better mapped in one-class than multi-class
520 settings. The performance of one-class methods in tracking changes was mixed and
521 more research should be carried out in the development of automated change detection
522 methods for specific single habitat types. Finally, applying one-class methods in
523 mapping the extent, distribution and dynamics of single habitat and land cover types at a
524 fine scale over a large spatial extent is a promising research avenue as low-cost VHRS
525 satellite images are becoming more widely available.

526 Acknowledgements: This research was supported by the Academy of Finland (projects 291736
527 and 296423).

528 **References**

- 529 Adam, Elhadi, Onesimo Mutanga, John Odindi, and Elfatih M Abdel-Rahman. 2014.
530 "Land-use/cover classification in a heterogeneous coastal landscape using
531 RapidEye imagery: evaluating the performance of random forest and support
532 vector machines classifiers." *International journal of remote sensing* 35
533 (10):3440-58.
- 534 Amici, V., M. Marcantonio, N. La Porta, and D. Rocchini. 2017. "A multi-temporal
535 approach in MaxEnt modelling: A new frontier for land use/land cover change
536 detection." *Ecological Informatics* 40:40-9. doi: 10.1016/j.ecoinf.2017.04.005.
- 537 Anderson, H. B., L. Nilsen, H. Tommervik, S. R. Karlsen, S. Nagai, and E. J. Cooper.
538 2016. "Using ordinary digital cameras in place of near-infrared sensors to derive
539 vegetation indices for phenology studies of high arctic vegetation." *Remote*
540 *Sensing* 8 (10). doi: 10.3390/rs8100847.
- 541 Andrew, M. E., and J. M. Shephard. 2017. "Semi-automated detection of eagle nests: an
542 application of very high-resolution image data and advanced image analyses to
543 wildlife surveys." *Remote Sensing in Ecology and Conservation* 3 (2):66-80.
544 doi: 10.1002/rse2.38.
- 545 Ao, Z., Y. Su, W. Li, Q. Guo, and J. Zhang. 2017. "One-class classification of airborne
546 LiDAR data in urban areas using a presence and background learning
547 algorithm." *Remote Sensing* 9 (10). doi: 10.3390/rs9101001.
- 548 Araya-López, R. A., J. Lopatin, F. E. Fassnacht, and H. J. Hernández. 2018.
549 "Monitoring Andean high altitude wetlands in central Chile with seasonal
550 optical data: A comparison between Worldview-2 and Sentinel-2 imagery."
551 *ISPRS Journal of Photogrammetry and Remote Sensing*. doi:
552 10.1016/j.isprsjprs.2018.04.001.
- 553 Baldeck, C. A., and G. P. Asner. 2015. "Single-Species Detection With Airborne
554 Imaging Spectroscopy Data: A Comparison of Support Vector Techniques."
555 *Ieee Journal of Selected Topics in Applied Earth Observations and Remote*
556 *Sensing* 8 (6):2501-12. doi: 10.1109/jstars.2014.2346475.
- 557 Baldeck, C. A., G. P. Asner, R. E. Martin, C. B. Anderson, D. E. Knapp, J. R. Kellner,
558 and S. J. Wright. 2015. "Operational Tree Species Mapping in a Diverse

559 Tropical Forest with Airborne Imaging Spectroscopy." *Plos One* 10 (7). doi:
560 10.1371/journal.pone.0118403.

561 Ballings, M., and D. Van der Poel. 2015. "rotationForest: Fit and Deploy Rotation
562 Forest Models." <http://CRAN.R-project.org/package=rotationForest>.

563 Barbosa, J. M., G. P. Asner, R. E. Martin, C. A. Baldeck, F. Hughes, and T. Johnson.
564 2016. "Determining Subcanopy Psidium cattleianum Invasion in Hawaiian
565 Forests Using Imaging Spectroscopy." *Remote Sensing* 8 (1). doi:
566 10.3390/rs8010033.

567 Bartsch, A., A. Hofler, C. Kroisleitner, and A. M. Trofaiher. 2016. "Land Cover Mapping
568 in Northern High Latitude Permafrost Regions with Satellite Data:
569 Achievements and Remaining Challenges." *Remote Sensing* 8 (12). doi:
570 10.3390/rs8120979.

571 Beck, I., R. Ludwig, M. Bernier, E. Lévesque, and J. Boike. 2015. "Assessing
572 Permafrost Degradation and Land Cover Changes (1986-2009) using Remote
573 Sensing Data over Umiujaq, Sub-Arctic Québec." *Permafrost and Periglacial
574 Processes* 26 (2):129-41. doi: 10.1002/ppp.1839.

575 Belgiu, M., and L. Dragut. 2016. "Random forest in remote sensing: A review of
576 applications and future directions." *ISPRS Journal of Photogrammetry and
577 Remote Sensing* 114:24-31. doi: 10.1016/j.isprsjprs.2016.01.011.

578 Belshe, E. F., E. A. G. Schuur, and G. Grosse. 2013. "Quantification of upland
579 thermokarst features with high resolution remote sensing." *Environmental
580 Research Letters* 8 (3). doi: 10.1088/1748-9326/8/3/035016.

581 Benz, U. C., P. Hofmann, G. Willhauck, I. Lingenfelder, and M. Heynen. 2004. "Multi-
582 resolution, object-oriented fuzzy analysis of remote sensing data for GIS-ready
583 information." *ISPRS Journal of Photogrammetry and Remote Sensing* 58 (3-
584 4):239-58. doi: 10.1016/j.isprsjprs.2003.10.002.

585 Blaschke, Thomas, Geoffrey J Hay, Maggi Kelly, Stefan Lang, Peter Hofmann,
586 Elisabeth Addink, Raul Queiroz Feitosa, Freek van der Meer, Harald van der
587 Werff, and Frieke van Coillie. 2014. "Geographic object-based image analysis-
588 towards a new paradigm." *ISPRS Journal of Photogrammetry and Remote
589 Sensing* 87:180-91.

590 Bockheim, J. G., and C. Tarnocai. 1998. "Recognition of cryoturbation for classifying
591 permafrost-affected soils." *Geoderma* 81 (3-4):281-93. doi: 10.1016/s0016-
592 7061(97)00115-8.

593 Borge, A. F., S. Westermann, I. Solheim, and B. Etzelmuller. 2017. "Strong degradation
594 of palsas and peat plateaus in northern Norway during the last 60 years."
595 *Cryosphere* 11 (1):1-16. doi: 10.5194/tc-11-1-2017.

596 Boyd, D. S., C. Sanchez-Hernandez, and G. M. Foody. 2006. "Mapping a specific class
597 for priority habitats monitoring from satellite sensor data." *International journal
598 of remote sensing* 27 (13):2631-44. doi: 10.1080/01431160600554348.

599 Breiman, L. 2001. "Random forests." *Machine Learning* 45 (1):5-32. doi:
600 10.1023/a:1010933404324.

601 Chavez, P. S. 1988. "An improved dark-object subtraction technique for atmospheric
602 scattering correction of multispectral data." *Remote Sensing of Environment* 24
603 (3):459-79. doi: 10.1016/0034-4257(88)90019-3.

604 Chen, C., A. Liaw, and L. Breiman. 2004. "Using Random Forest to Learn Imbalanced
605 Data." In *Statistics Technical Reports*. Berkeley, CA, USA: University of
606 California Berkeley.

- 607 Chen, X. H., D. M. Yin, J. Chen, and X. Cao. 2016. "Effect of training strategy for
608 positive and unlabelled learning classification: test on Landsat imagery."
609 *Remote Sensing Letters* 7 (11):1063-72. doi: 10.1080/2150704x.2016.1217437.
- 610 Chignell, S. M., M. W. Luizza, S. Skach, N. E. Young, and P. H. Evangelista. 2018.
611 "An integrative modeling approach to mapping wetlands and riparian areas in a
612 heterogeneous Rocky Mountain watershed." *Remote Sensing in Ecology and*
613 *Conservation* 4 (2):150-65. doi: 10.1002/rse2.63.
- 614 Coops, N. C., M. Johnson, M. A. Wulder, and J. C. White. 2006. "Assessment of
615 QuickBird high spatial resolution imagery to detect red attack damage due to
616 mountain pine beetle infestation." *Remote Sensing of Environment* 103 (1):67-
617 80. doi: 10.1016/j.rse.2006.03.012.
- 618 Deng, X., W. Li, X. Liu, Q. Guo, and S. Newsam. 2018. "One-class remote sensing
619 classification: One-class vs. Binary classifiers." *International journal of remote*
620 *sensing* 39 (6):1890-910. doi: 10.1080/01431161.2017.1416697.
- 621 Du, P. J., A. Samat, B. Waske, S. C. Liu, and Z. H. Li. 2015. "Random Forest and
622 Rotation Forest for fully polarized SAR image classification using polarimetric
623 and spatial features." *ISPRS Journal of Photogrammetry and Remote Sensing*
624 105:38-53. doi: 10.1016/j.isprsjprs.2015.03.002.
- 625 Duro, Dennis C, Steven E Franklin, and Monique G Dubé. 2012. "A comparison of
626 pixel-based and object-based image analysis with selected machine learning
627 algorithms for the classification of agricultural landscapes using SPOT-5 HRG
628 imagery." *Remote Sensing of Environment* 118:259-72.
- 629 Elith, J., S. J. Phillips, T. Hastie, M. Dudík, Y. E. Chee, and C. J. Yates. 2011. "A
630 statistical explanation of MaxEnt for ecologists." *Diversity and Distributions* 17
631 (1):43-57. doi: 10.1111/j.1472-4642.2010.00725.x.
- 632 Elmendorf, S. C., G. H. R. Henry, R. D. Hollister, R. G. Bjork, N. Boulanger-Lapointe,
633 E. J. Cooper, J. H. C. Cornelissen, et al. 2012. "Plot-scale evidence of tundra
634 vegetation change and links to recent summer warming." *Nature Climate*
635 *Change* 2 (6):453-7. doi: 10.1038/nclimate1465.
- 636 Haralick, R. M., I. Dinstein, and K. Shanmugam. 1973. "Textural Features for Image
637 Classification." *IEEE Transactions on Systems, Man and Cybernetics* SMC-3
638 (6):610-21. doi: 10.1109/TSMC.1973.4309314.
- 639 Hugelius, G., J. Routh, P. Kuhry, and P. Crill. 2012. "Mapping the degree of
640 decomposition and thaw remobilization potential of soil organic matter in
641 discontinuous permafrost terrain." *Journal of Geophysical Research:*
642 *Biogeosciences* 117 (2). doi: 10.1029/2011JG001873.
- 643 Jorgenson, M. T., and G. Grosse. 2016. "Remote Sensing of Landscape Change in
644 Permafrost Regions." *Permafrost and Periglacial Processes* 27 (4):324-38. doi:
645 10.1002/ppp.1914.
- 646 Juutinen, S., T. Virtanen, V. Kondratyev, T. Laurila, M. Linkosalmi, J. Mikola, J.
647 Nyman, A. Räsänen, J-P. Tuovinen, and M. Aurela. 2017. "Spatial variation and
648 seasonal dynamics of leaf-area index in the arctic tundra-implications for linking
649 ground observations and satellite images." *Environmental Research Letters*
650 12:095002. doi: https://doi.org/10.1088/1748-9326/aa7f85.
- 651 Kavzoglu, T., and I. Colkesen. 2013. "An assessment of the effectiveness of a rotation
652 forest ensemble for land-use and land-cover mapping." *International journal of*
653 *remote sensing* 34 (12):4224-41. doi: 10.1080/01431161.2013.774099.
- 654 Kursu, M. B., and W. R. Rudnicki. 2010. "Feature Selection with the Boruta Package."
655 *Journal of Statistical Software* 36 (11):1-13.

- 656 Laidler, G. J., and P. Treitz. 2003. "Biophysical remote sensing of arctic environments."
657 *Progress in Physical Geography* 27 (1):44-68. doi:
658 10.1191/0309133303pp358ra.
- 659 Li, J., M. Tran, and J. Siwabessy. 2016. "Selecting Optimal Random Forest Predictive
660 Models: A Case Study on Predicting the Spatial Distribution of Seabed
661 Hardness." *Plos One* 11 (2). doi: 10.1371/journal.pone.0149089.
- 662 Li, P., and H. Xu. 2010. "Land-cover change detection using one-class support vector
663 machine." *Photogrammetric Engineering and Remote Sensing* 76 (3):255-63.
- 664 Li, W., Q. Guo, and C. Elkan. 2011. "A positive and unlabeled learning algorithm for
665 one-class classification of remote-sensing data." *Ieee Transactions on
666 Geoscience and Remote Sensing* 49 (2):717-25. doi:
667 10.1109/TGRS.2010.2058578.
- 668 Li, W. K., and Q. H. Guo. 2010. "A maximum entropy approach to one-class
669 classification of remote sensing imagery." *International journal of remote
670 sensing* 31 (8):2227-35. doi: 10.1080/01431161003702245.
- 671 Li, X. J., W. T. Chen, X. W. Cheng, and L. Z. Wang. 2016. "A Comparison of Machine
672 Learning Algorithms for Mapping of Complex Surface-Mined and Agricultural
673 Landscapes Using ZiYuan-3 Stereo Satellite Imagery." *Remote Sensing* 8 (6).
674 doi: 10.3390/rs8060514.
- 675 Liaw, A., and M. Wiener. 2002. "Classification and Regression by randomForest." *R
676 News* 2 (3):18-22.
- 677 Lin, J., X. Liu, K. Li, and X. Li. 2014. "A maximum entropy method to extract urban
678 land by combining MODIS reflectance, MODIS NDVI, and DMSP-OLS data."
679 *International journal of remote sensing* 35 (18):6708-27. doi:
680 10.1080/01431161.2014.960623.
- 681 Liu, B., Y. Dai, X. Li, W. S. Lee, and P. S. Yu. 2003. Building Text Classifiers Using
682 Positive and Unlabeled Examples. Paper presented at the Proceedings of the
683 Third IEEE International Conference on Data Mining (ICDM '03).
- 684 Liu, R., W. Li, X. Liu, X. Lu, T. Li, and Q. Guo. 2018. "An Ensemble of Classifiers
685 Based on Positive and Unlabeled Data in One-Class Remote Sensing
686 Classification." *Ieee Journal of Selected Topics in Applied Earth Observations
687 and Remote Sensing* 11 (2):572-84. doi: 10.1109/JSTARS.2017.2789213.
- 688 Low, F., U. Michel, S. Dech, and C. Conrad. 2013. "Impact of feature selection on the
689 accuracy and spatial uncertainty of per-field crop classification using Support
690 Vector Machines." *ISPRS Journal of Photogrammetry and Remote Sensing*
691 85:102-19. doi: 10.1016/j.isprsjprs.2013.08.007.
- 692 Mack, B., R. Roscher, S. Stenzel, H. Feilhauer, S. Schmidlein, and B. Waske. 2016.
693 "Mapping raised bogs with an iterative one-class classification approach."
694 *ISPRS Journal of Photogrammetry and Remote Sensing* 120:53-64. doi:
695 10.1016/j.isprsjprs.2016.07.008.
- 696 Mack, B., R. Roscher, and B. Waske. 2014. "Can I Trust My One-Class Classification?"
697 *Remote Sensing* 6 (9):8779-802. doi: 10.3390/rs6098779.
- 698 Mack, B., and B. Waske. 2017. "In-depth comparisons of MaxEnt, biased SVM and
699 one-class SVM for one-class classification of remote sensing data." *Remote
700 Sensing Letters* 8 (3):290-9. doi: 10.1080/2150704x.2016.1265689.
- 701 Marushchak, M. E., I. Kiepe, C. Biasi, V. Elsakov, T. Friborg, T. Johansson, H.
702 Soegaard, T. Virtanen, and P. J. Martikainen. 2013. "Carbon dioxide balance of
703 subarctic tundra from plot to regional scales." *Biogeosciences* 10 (1):437-52.
704 doi: 10.5194/bg-10-437-2013.

705 Marushchak, M. E., A. Pitkämäki, H. Koponen, C. Biasi, M. Seppälä, and P. J.
706 Martikainen. 2011. "Hot spots for nitrous oxide emissions found in different
707 types of permafrost peatlands." *Global Change Biology* 17 (8):2601-14. doi:
708 10.1111/j.1365-2486.2011.02442.x.

709 McCarthy, M. J., and J. N. Halls. 2014. "Habitat mapping and change assessment of
710 coastal environments: An examination of worldview-2, quickbird, and ikonos
711 satellite imagery and airborne lidar for mapping barrier island habitats." *ISPRS
712 International Journal of Geo-Information* 3 (1):297-325. doi:
713 10.3390/ijgi3010297.

714 McFeeters, S. K. 1996. "The use of the Normalized Difference Water Index (NDWI) in
715 the delineation of open water features." *International journal of remote sensing*
716 17 (7):1425-32. doi: 10.1080/01431169608948714.

717 Mountrakis, G., J. Im, and C. Ogole. 2011. "Support vector machines in remote sensing:
718 A review." *ISPRS Journal of Photogrammetry and Remote Sensing* 66 (3):247-
719 59. doi: 10.1016/j.isprsjprs.2010.11.001.

720 Myers-Smith, I. H., S. C. Elmendorf, P. S. A. Beck, M. Wilmking, M. Hallinger, D.
721 Blok, K. D. Tape, et al. 2015. "Climate sensitivity of shrub growth across the
722 tundra biome." *Nature Climate Change* 5 (9):887-+. doi: 10.1038/nclimate2697.

723 Novack, T., T. Esch, H. Kux, and U. Stilla. 2011. "Machine learning comparison
724 between WorldView-2 and QuickBird-2-simulated imagery regarding object-
725 based urban land cover classification." *Remote Sensing* 3 (10):2263-82. doi:
726 10.3390/rs3102263.

727 Noviello, M., B. Cafarelli, C. Calculli, A. Sarris, and P. Mairota. 2018. "Investigating
728 the distribution of archaeological sites: Multiparametric vs probability models
729 and potentials for remote sensing data." *Applied Geography* 95:34-44. doi:
730 10.1016/j.apgeog.2018.04.005.

731 Obu, J., H. Lantuit, I. Myers-Smith, B. Heim, J. Wolter, and M. Fritz. 2017. "Effect of
732 terrain characteristics on soil organic carbon and total nitrogen stocks in soils of
733 Herschel Island, western Canadian Arctic." *Permafrost and Periglacial
734 Processes* 28 (1):92-107. doi: 10.1002/ppp.1881.

735 Pacifici, F., M. Chini, and W. J. Emery. 2009. "A neural network approach using multi-
736 scale textural metrics from very high-resolution panchromatic imagery for urban
737 land-use classification." *Remote Sensing of Environment* 113 (6):1276-92. doi:
738 10.1016/j.rse.2009.02.014.

739 Pau, G., F. Fuchs, O. Sklyar, M. Boutros, and W. Huber. 2010. "EBImage-an R package
740 for image processing with applications to cellular phenotypes." *Bioinformatics*
741 26 (7):979-81. doi: 10.1093/bioinformatics/btq046.

742 Peterson, R. A., and W. B. Krantz. 2003. "A mechanism for differential frost heave and
743 its implications for patterned-ground formation." *Journal of Glaciology* 49
744 (164):69-80. doi: 10.3189/172756503781830854.

745 Pflugmacher, D., O. N. Krankina, W. B. Cohen, M. A. Friedl, D. Sulla-Menashe, R. E.
746 Kennedy, P. Nelson, et al. 2011. "Comparison and assessment of coarse
747 resolution land cover maps for Northern Eurasia." *Remote Sensing of
748 Environment* 115 (12):3539-53. doi: 10.1016/j.rse.2011.08.016.

749 Phillips, S. J., R. P. Anderson, and R. E. Schapire. 2006. "Maximum entropy modeling
750 of species geographic distributions." *Ecological Modelling* 190 (3-4):231-59.
751 doi: 10.1016/j.ecolmodel.2005.03.026.

752 Poona, N. K., A. van Niekerk, R. L. Nadel, and R. Ismail. 2016. "Random Forest (RF)
753 Wrappers for Waveband Selection and Classification of Hyperspectral Data."
754 *Applied Spectroscopy* 70 (2):322-33. doi: 10.1177/0003702815620545.

755 R Core Team. 2015. "R: A language and environment for statistical computing." R
756 Foundation for Statistical Computing. <https://www.R-project.org/>.

757 Rasanen, A., M. Kuitunen, E. Tomppo, and A. Lensu. 2014. "Coupling high-resolution
758 satellite imagery with ALS-based canopy height model and digital elevation
759 model in object-based boreal forest habitat type classification." *ISPRS Journal
760 of Photogrammetry and Remote Sensing* 94:169-82. doi:
761 10.1016/j.isprsjprs.2014.05.003.

762 Repo, M. E., S. Susiluoto, S. E. Lind, S. Jokinen, V. Elsakov, C. Biasi, T. Virtanen, and
763 P. J. Martikainen. 2009. "Large N₂O emissions from cryoturbated peat soil in
764 tundra." *Nature Geoscience* 2 (3):189-92. doi: 10.1038/ngeo434.

765 Rodriguez-Galiano, Victor Francisco, Bardan Ghimire, John Rogan, Mario Chica-
766 Olmo, and Juan Pedro Rigol-Sanchez. 2012. "An assessment of the effectiveness
767 of a random forest classifier for land-cover classification." *ISPRS Journal of
768 Photogrammetry and Remote Sensing* 67:93-104.

769 Rodriguez, J. J., and L. I. Kuncheva. 2006. "Rotation forest: A new classifier ensemble
770 method." *Ieee Transactions on Pattern Analysis and Machine Intelligence* 28
771 (10):1619-30. doi: 10.1109/tpami.2006.211.

772 Rouse, J. W. Jr., R. H. Haas, J. A. Schell, and D. W. Deering. 1973. "Monitoring
773 vegetation systems in the Great Plains with ERTS." In *Third Earth Resources
774 Technology Satellite-1 Symposium*, 309-17. Washington, DC: NASA.

775 Räsänen, Aleksi, Antti Rusanen, Markku Kuitunen, and Anssi Lensu. 2013. "What
776 makes segmentation good? A case study in boreal forest habitat mapping."
777 *International journal of remote sensing* 34 (23):8603-27.

778 Samsudin, S. H., H. Z. M. Shafri, A. Hamedianfar, and S. Mansor. 2015. "Spectral
779 feature selection and classification of roofing materials using field spectroscopy
780 data." *Journal of Applied Remote Sensing* 9. doi: 10.1117/1.jrs.9.095079.

781 Sanchez-Hernandez, C., D. S. Boyd, and G. M. Foody. 2007. "Mapping specific
782 habitats from remotely sensed imagery: Support vector machine and support
783 vector data description based classification of coastal saltmarsh habitats."
784 *Ecological Informatics* 2 (2):83-8. doi: 10.1016/j.ecoinf.2007.04.003.

785 Sannel, A. B. K., and P. Kuhry. 2011. "Warming-induced destabilization of peat
786 plateau/thermokarst lake complexes." *Journal of Geophysical Research:
787 Biogeosciences* 116 (3). doi: 10.1029/2010JG001635.

788 Schölkopf, B., R. Williamson, A. Smola, J. Shawe-Taylor, and J. Piatt. 2000. Support
789 vector method for novelty detection. Paper presented at the Advances in Neural
790 Information Processing Systems.

791 Segal, R. A., T. C. Lantz, and S. V. Kokelj. 2016. "Acceleration of thaw slump activity
792 in glaciated landscapes of the Western Canadian Arctic." *Environmental
793 Research Letters* 11 (3). doi: 10.1088/1748-9326/11/3/034025.

794 Seppälä, M. 2003. "Surface abrasion of palsas by wind action in Finnish Lapland."
795 *Geomorphology* 52 (1-2):141-8. doi: 10.1016/S0169-555X(02)00254-4.

796 Singh, Ashbindu. 1989. "Review article digital change detection techniques using
797 remotely-sensed data." *International journal of remote sensing* 10 (6):989-
798 1003.

799 Song, B. Q., P. J. Li, J. Li, and A. Plaza. 2016. "One-Class Classification of Remote
800 Sensing Images Using Kernel Sparse Representation." *Ieee Journal of Selected
801 Topics in Applied Earth Observations and Remote Sensing* 9 (4):1613-23. doi:
802 10.1109/jstars.2015.2508285.

- 803 Stenzel, S., F. E. Fassnacht, B. Mack, and S. Schmidtlein. 2017. "Identification of high
804 nature value grassland with remote sensing and minimal field data." *Ecological*
805 *Indicators* 74:28-38. doi: 10.1016/j.ecolind.2016.11.005.
- 806 Stenzel, S., H. Feilhauer, B. Mack, A. Metz, and S. Schmidtlein. 2014. "Remote sensing
807 of scattered Natura 2000 habitats using a one-class classifier." *International*
808 *Journal of Applied Earth Observation and Geoinformation* 33:211-7. doi:
809 10.1016/j.jag.2014.05.012.
- 810 Stow, D. A., A. Hope, D. McGuire, D. Verbyla, J. Gamon, F. Huemmrich, S. Houston,
811 et al. 2004. "Remote sensing of vegetation and land-cover change in Arctic
812 Tundra Ecosystems." *Remote Sensing of Environment* 89 (3):281-308. doi:
813 10.1016/j.rse.2003.10.018.
- 814 Tape, K., M. Sturm, and C. Racine. 2006. "The evidence for shrub expansion in
815 Northern Alaska and the Pan-Arctic." *Global Change Biology* 12 (4):686-702.
816 doi: 10.1111/j.1365-2486.2006.01128.x.
- 817 Tewkesbury, Andrew P, Alexis J Comber, Nicholas J Tate, Alistair Lamb, and Peter F
818 Fisher. 2015. "A critical synthesis of remotely sensed optical image change
819 detection techniques." *Remote Sensing of Environment* 160:1-14.
- 820 Wang, P., L. Mommer, J. van Ruijven, F. Berendse, T. C. Maximov, and Mmpd
821 Heijmans. 2016. "Seasonal changes and vertical distribution of root standing
822 biomass of graminoids and shrubs at a Siberian tundra site." *Plant and Soil* 407
823 (1-2):55-65. doi: 10.1007/s11104-016-2858-5.
- 824 Vapnik, V. 1982. *Estimation of Dependences Based on Empirical Data*. Vol. 40. New
825 York: Springer-Verlag.
- 826 Vert, J.-P., K. Tsuda, and B. Schölkopf. 2004. "A primer on kernel methods." In *Kernel*
827 *Methods in Computational Biology*, edited by B. Schölkopf, K. Tsuda and J.-P.
828 Vert, 35-70. Cambridge, MA, USA: MIT Press.
- 829 Westermann, S., C. R. Duguay, G. Grosse, and A. Kääb. 2014. "Remote sensing of
830 permafrost and frozen ground." In *Remote Sensing of the Cryosphere*, 307-44.
- 831 Virtanen, T., and M. Ek. 2014. "The fragmented nature of tundra landscape."
832 *International Journal of Applied Earth Observation and Geoinformation* 27:4-
833 12. doi: 10.1016/j.jag.2013.05.010.
- 834 Voigt, C., R. E. Lamprecht, M. E. Marushchak, S. E. Lind, A. Novakovskiy, M. Aurela,
835 P. J. Martikainen, and C. Biasi. 2016. "Warming of subarctic tundra increases
836 emissions of all three important greenhouse gases - carbon dioxide, methane,
837 and nitrous oxide." *Global Change Biology*. doi: 10.1111/gcb.13563.
- 838 Väiliranta, M., M. Marushchak, J.-P. Tuovinen, A. Lohila, C. Biasi, T. Ronkainen, H.
839 Zhang, et al. 2018. "Increased climate forcing of high-latitude peatlands due to
840 permafrost initiation." *Submitted manuscript*.
- 841 Xu, X., X. Liu, X. Li, Q. Xin, Y. Chen, Q. Shi, and B. Ai. 2016. "Global snow cover
842 estimation with Microwave Brightness Temperature measurements and one-
843 class in situ observations." *Remote Sensing of Environment* 182:227-51. doi:
844 10.1016/j.rse.2016.05.010.
- 845 Yu, Q., H. Epstein, R. Engstrom, and D. Walker. 2017. "Circumpolar arctic tundra
846 biomass and productivity dynamics in response to projected climate change and
847 herbivory." *Global Change Biology*. doi: 10.1111/gcb.13632.

848

849

850 Table 1. *F*-scores of the different classifiers using the parameter combinations yielding
851 highest *F*-score values. Values are calculated based on two different evaluations: (1)
852 out-of-bag (RF) or tenfold cross-validation (other classifiers) estimates using the
853 training data only, or (2) using independent test data. The highest *F*-scores for each
854 image and classification setting are marked in bold.

Evaluation	Classification	Binary				Positive and unlabelled			
		OCSVM	BSVM	RF	ROF	OCSVM	BSVM	RF	ROF
Training data cross-validation	QB	0.85	0.89	0.88	0.94	0.90	0.93	0.94	0.96
	WV-3LR	0.87	0.92	0.92	0.93	0.95	0.96	0.96	0.96
	WV-3HR	0.77	0.86	0.86	0.91	0.88	0.90	0.90	0.95
Independent test data	QB	0.48	0.39	0.48	0.40	0.44	0.45	0.46	0.42
	WV-3LR	0.32	0.31	0.38	0.22	0.42	0.45	0.42	0.34
	WV-3HR	0.42	0.48	0.57	0.52	0.43	0.56	0.48	0.53

855 Table 2. Classification accuracy results for the QB classifications. The best
856 performances for the binary and PU settings are marked in bold.

Performance metric	Binary				PU			
	OCSVM	BSVM	RF	ROF	OCSVM	BSVM	RF	ROF
User's accuracy (%)	36.9	46.7	43.7	39.2	34.8	42.0	46.8	58.9
Segment that is 50% correct (%)	41.7	63.2	54.7	57.4	39.2	54.5	63.0	84.6
Segment that is 10% correct (%)	80.6	92.1	88.7	68.1	74.7	81.8	91.3	100.0
Producer's accuracy (%)	60.0	42.4	53.7	43.4	59.8	21.5	50.0	34.4
Reference area that is 50% mapped (%)	56.2	37.1	49.4	31.5	56.2	18.0	42.7	25.8
Reference area that is 10% mapped (%)	65.2	40.4	52.8	34.8	65.2	19.1	46.1	29.2
Number of segment classified as bare peat	72	38	53	47	79	22	46	26
Number of bare peat area in the reference	89	89	89	89	89	89	89	89
Mapped area (ha)	0.866	0.472	0.643	0.580	0.914	0.267	0.558	0.308
Bare peat area in the reference (ha)	0.521	0.521	0.521	0.521	0.521	0.521	0.521	0.521
Number of segment total	636	455	418	437	741	291	436	290
Total (ha)	9.102	6.686	5.939	6.231	10.030	4.364	6.070	4.311

857

858

859 Table 3. Classification accuracy results for the WV-3LR classifications. The best
 860 performances for the binary and PU settings are marked in bold.

Performance metric	Binary				PU			
	OCSVM	BSVM	RF	ROF	OCSVM	BSVM	RF	ROF
User's accuracy (%)	31.7	25.7	54.2	21.8	43.0	45.1	45.8	45.0
Segment that is 50% correct (%)	34.9	46.8	58.6	33.3	44.7	48.1	48.9	53.1
Segment that is 10% correct (%)	72.1	72.3	82.8	52.4	83.0	78.8	77.8	78.1
Producer's accuracy (%)	31.3	37.7	28.9	22.6	40.7	45.1	38.6	27.7
Reference area that is 50% mapped (%)	30.3	33.7	22.5	20.2	37.1	39.3	33.7	23.6
Reference area that is 10% mapped (%)	36.0	38.2	25.8	22.5	41.6	44.9	38.2	27.0
Number of segment classified as bare peat	43	47	29	42	47	52	45	32
Number of bare peat area in the reference	89	89	89	89	89	89	89	89
Mapped area (ha)	0.520	0.772	0.279	0.544	0.503	0.526	0.443	0.323
Bare peat area in the reference (ha)	0.521	0.521	0.521	0.521	0.521	0.521	0.521	0.521
Number of segment total	339	390	288	424	365	395	368	314
Total (ha)	4.674	7.942	4.069	5.905	4.746	5.469	5.369	4.306

861

862

863 Table 4. Classification accuracy results for the WV-3HR classifications. The best
 864 performances for the binary and PU settings are marked in bold.

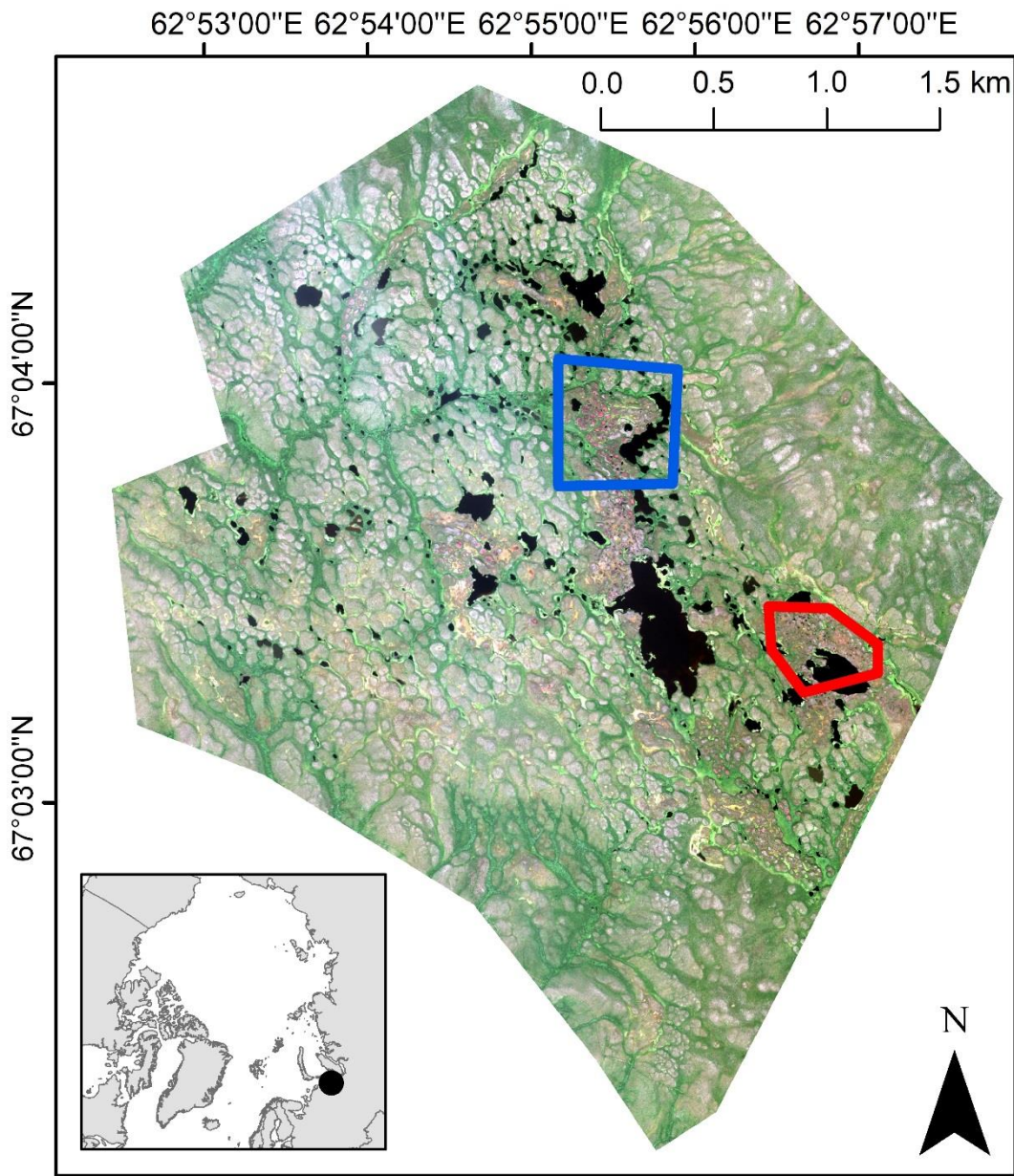
Performance metric	Binary				PU			
	OCSVM	BSVM	RF	ROF	OCSVM	BSVM	RF	ROF
User's accuracy (%)	42.9	63.6	56.8	58.2	33.7	55.4	47.2	49.1
Segment that is 50% correct (%)	50.7	76.5	66.3	69.6	40.2	65.8	54.1	61.4
Segment that is 10% correct (%)	80.0	88.2	89.5	84.1	68.2	92.4	83.5	86.4
Producer's accuracy (%)	40.6	38.4	57.4	47.3	59.9	55.7	49.2	56.8
Reference area that is 50% mapped (%)	43.8	32.6	56.2	41.6	65.2	53.9	53.9	58.4
Reference area that is 10% mapped (%)	55.1	46.1	68.5	52.8	79.8	62.9	67.4	66.3
Number of segment classified as bare peat	75	51	86	69	132	80	85	88
Number of bare peat area in the reference	89	89	89	89	89	89	89	89
Mapped area (ha)	0.498	0.318	0.531	0.427	0.930	0.528	0.550	0.606
Bare peat area in the reference (ha)	0.521	0.521	0.521	0.521	0.521	0.521	0.521	0.521
Number of segment total	513	319	454	359	951	604	685	549
Total (ha)	4.661	5.802	4.487	4.634	7.780	5.045	5.478	4.644

865

866

867 Table 5. Change detection metrics based on the QB and WV-3LR classifications.

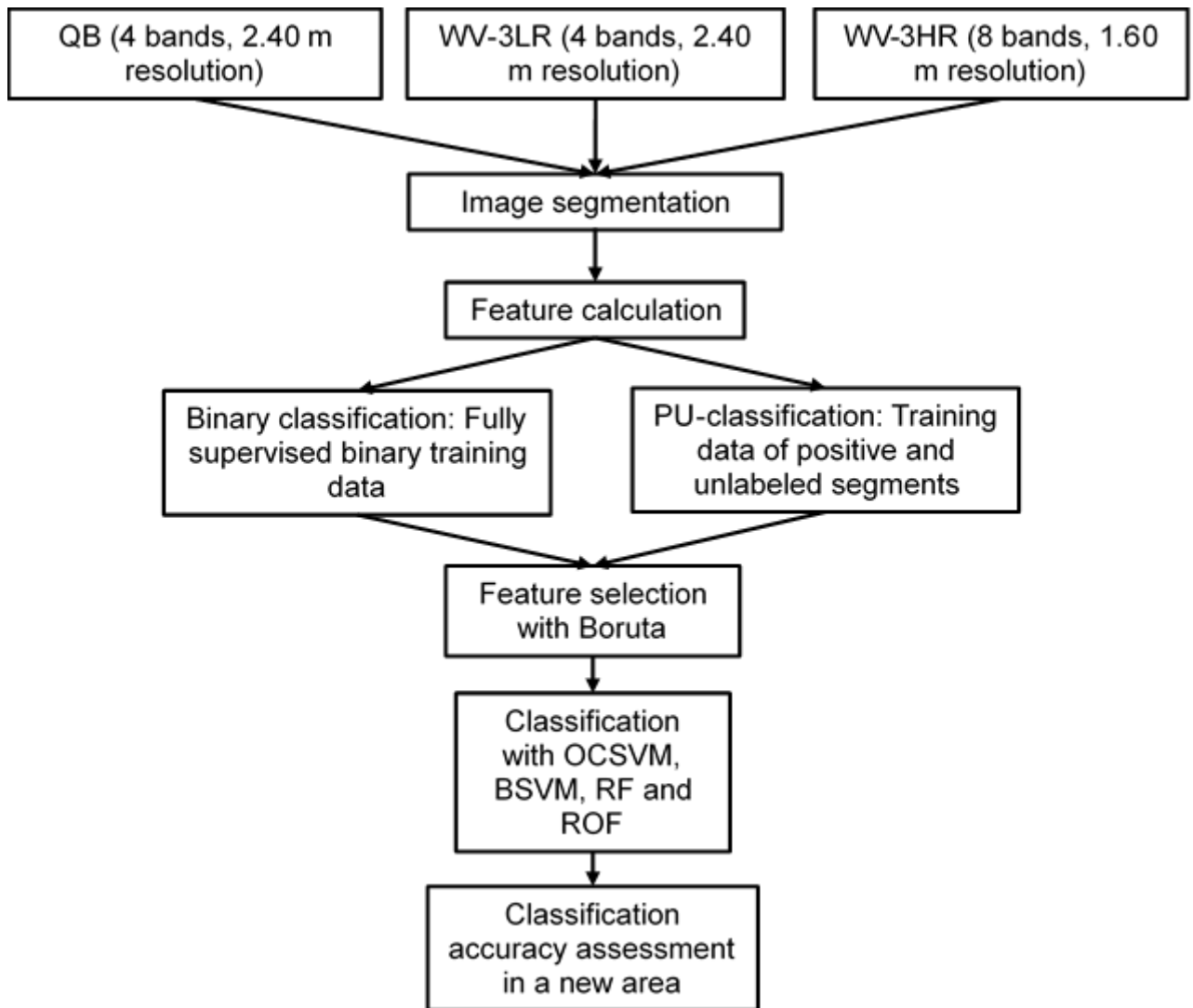
Metric	QB		WV-3LR		Decrease (%)	
	Area (ha)	Number of patches	Area (ha)	Number of patches	Area	Number of patches
Consensus of 7 classifiers	4.3	286	3.1	236	27.9	17.5
Consensus of 5 classifiers	5.7	401	4.4	318	22.8	20.7
Consensus of 3 classifiers	8.4	616	5.2	375	38.1	39.1
Lowest estimate	4.3	290	4.1	288	4.7	0.7
Average	7.0	487	5.3	360	24.3	26.1
Highest estimate	10.0	741	7.9	424	21.0	42.8



868

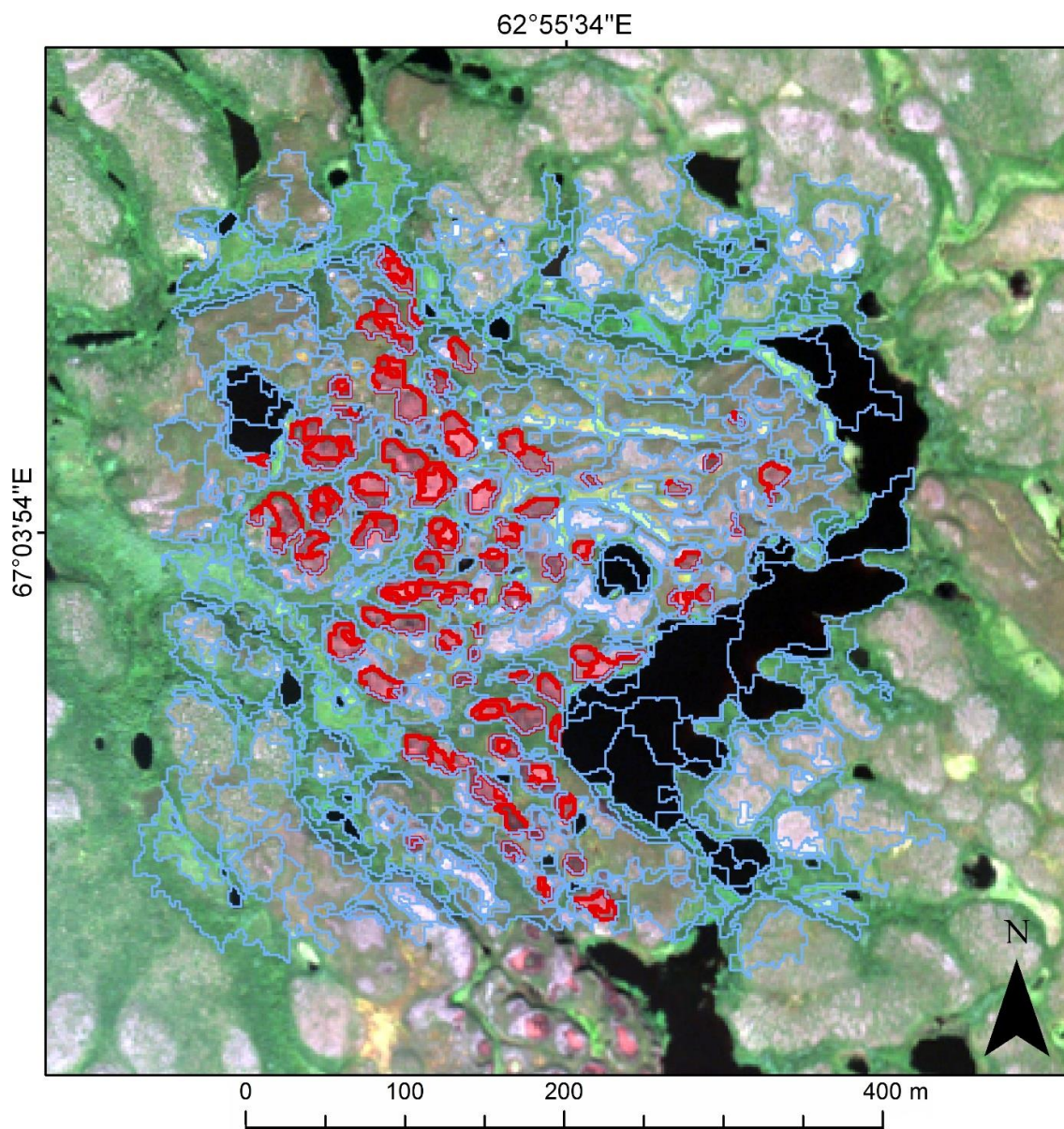
869 Figure 1. The study area and its location. The classifier training area is marked in blue

870 and the test area in red. Image: WorldView-3 ©DigitalGlobe.



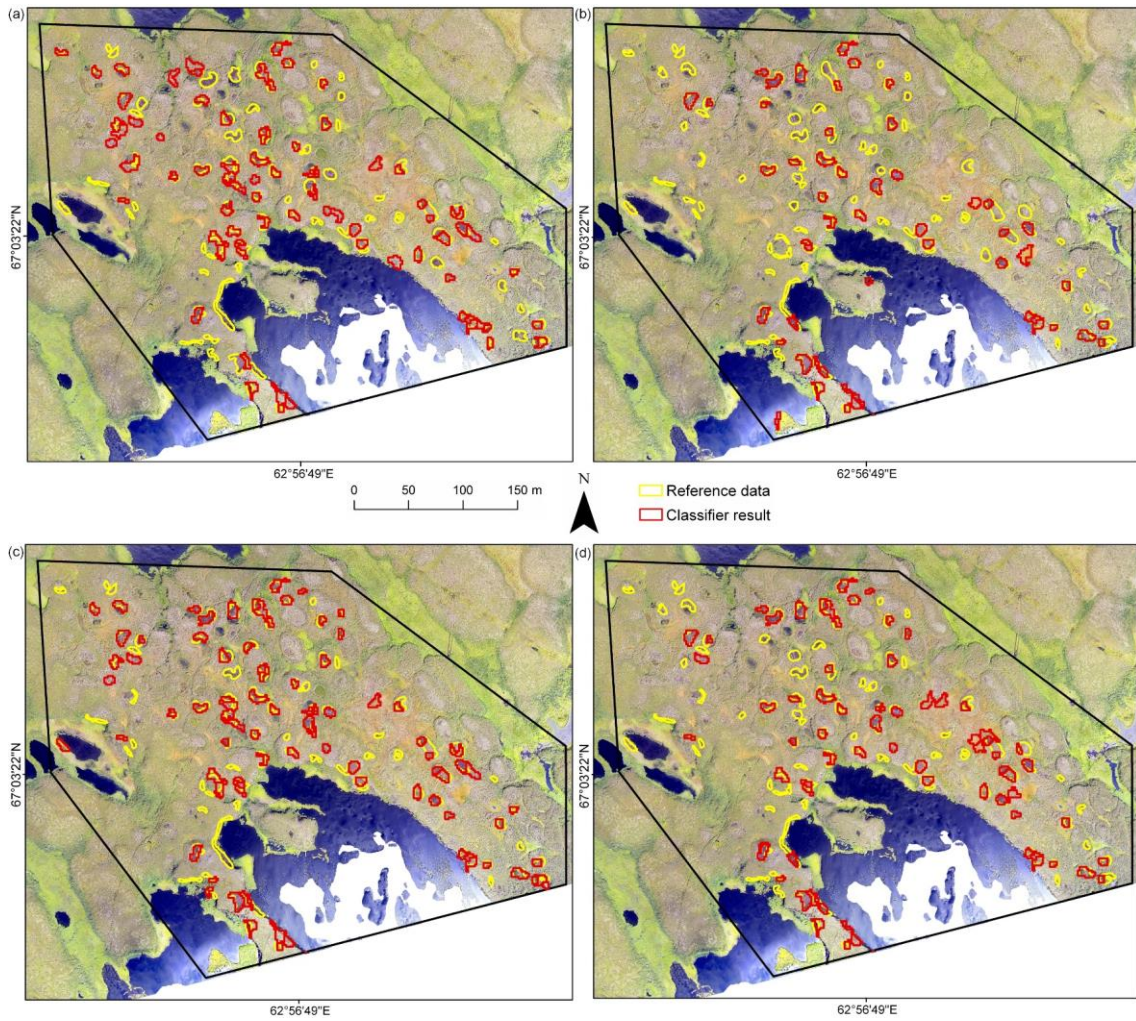
871

872 Figure 2. The workflow of the methods used.



873

874 Figure 3. The training area for the WV-3HR classifications. Bare peat areas were used
875 both in binary and positive and unlabelled settings and other land cover types in the
876 binary setting. Image ©DigitalGlobe.



877

878 Figure 4. Visualizations of the OCSVM (a), BSVM (b), RF (c), and ROF (d)

879 classifications for the WV-3HR classifications using the binary setting. Background

880 image: drone image from the validation area.

881